AD723160

AQCD-9352.1-D

a report

from the Texas A&M
RESEARCH FOUNDATION
College Station, Texas

49

Semi-Annual Technical Report

ARPA Order Numer - 1562

Grant Number - DA-ARO-D-31-124-71-G49

Program Code Number - 0D10

Principal Investigator - Dr. J. L. Stone
(713)845-7441

Name of Grantee - Texas A&M Research Foundation

Project Scientist - (See Principal Investigator)

Effective Date of Grant - January 1, 1971

Title of Work - Characterization of Conduction Processes in Amorphous Semiconductors

Grant Expiration Date - June 30, 1972

Amount of Grant - $50,015.00

Sponsored by

Advanced Research Projects Agency
ARPA Order No. 1562

CHAPTER I

THE PHOTODIELECTRIC EFFECT

1.1 Introduction

The conductivity of semiconductors lies between that of good conductors and good insulators and is determined in part by temperature and free carrier density. At liquid helium temperature (4.2°K) an intrinsic semiconductor sample can be described as an insulator except for the fact that the valence band electrons are bound much less tightly than those of a good insulator. This provides the possibility that one or more electrons can gain enough thermal energy to move into the conduction band.

In well established material properties studies Arndt, Hartwig and Stone[1]) and Hartwig and Hinds[2]) have shown that the complex conductivity of semiconductors can be effectively changed by photo-induced free carrier creation. Irradiation, hv, greater than the ionization energy produced free carriers at the expense of bound charges. These free

carriers, created as electron-hole pairs, add to the conductivity of the material for a length of time determined by the created carrier lifetime.

The photodielectric effect is a decrease in the real part of the complex dielectric constant as explained by Stone[3]. This decrease results from a phase shift in the velocity of the free carriers interacting with the microwave electric field. This can be characterized by a complex conductivity or mobility.

1.2 Cavity Perturbation

A method of measuring small changes in the dielectric constant of a material is to use such changes in the material to perturb the inherent field patterns of a resonant cavity. According to cavity perturbation theory, when the sample is excited by light photons, a change in the dielectric constant of the material will effect a change in the cavity Q and resonant frequency.

The complex angular frequency for a resonant cavity is

$$\omega = \omega_r + j\omega_i \tag{1.1}$$

where

ω_r = real component

ω_i = imaginary component

Sucher and Fox[4]) derive the following equation for the frequency perturbation of a resonant cavity.

$$\frac{\delta\omega}{\omega_2} = \frac{\omega_2-\omega_1}{\omega_2} \approx \frac{fr_2-fr_1}{fr_2} + j\left(\frac{1}{2Q_1} - \frac{1}{2Q_1}\right) \tag{1.2}$$

In this equation ω_1 is the resonant frequency of the cavity loaded with an unexcited sample and ω_2 is the resonant frequency after the sample has been excited. Thus, through the above equation, it can be seen that cavity perturbation contains both a change in the resonant frequency and a change in the cavity Q.

Starting with Maxwell's equations

$$\begin{aligned} \bar{\nabla} \times \bar{E} &= -j\omega\mu\bar{H} \\ \bar{\nabla} \times \bar{H} &= j\omega\varepsilon\bar{E} \end{aligned} \tag{1.3}$$

Stone [3] shows the relative frequency change due to dielectric samples to be

$$\frac{\omega_1-\omega_0}{\omega_1} = \frac{\Delta\omega_1}{\omega_1} = \frac{\int_{vc}(\varepsilon_0-\varepsilon_1)\bar{E}_0\cdot\bar{E}_1 d\bar{V} - \int_{vc}(\mu_0-\mu_1)\bar{H}_0\cdot\bar{H}_1 dV}{\int_{vc}(\varepsilon_0\bar{E}_0\cdot\bar{E}_1-\mu_0\bar{H}_0\cdot\bar{H}_1)dV} \tag{1.4}$$

$$\frac{\omega_2-\omega_0}{\omega_2} = \frac{\Delta\omega_2}{\omega_2} = \frac{\int_{vc}(\varepsilon_0-\varepsilon_2)\bar{E}_0\cdot\bar{E}_2 d\bar{V} - \int_{vc}(\mu_0-\mu_2)\bar{H}_0\cdot\bar{H}_2 dV}{\int_{vc}(\varepsilon_0\bar{E}_0\cdot\bar{E}_2-\mu_0\bar{H}_0\cdot\bar{H}_2)dV} \tag{1.5}$$

where the subscript "0" denotes the cavity with no sample, the subscript "1" denotes the cavity with an unexcited dielectric sample and subscript "2" denotes the cavity with the sample excited by light. These are the general perturbation equations that describe a change in resonant cavity frequency. Frequency shifts caused by exciting the sample with light are considered as perturbations on the original perturbations caused by loading the cavity with the sample. The assumptions made in the derivation of the above equations are that the sample volume, V_s, is much smaller than the cavity volume, V_c, and that

in the cavity, $\mu_0=\mu_1=\mu_2$ and $\epsilon_0=\epsilon_1=\epsilon_2$ everywhere except in the sample.

If the sample is placed in a position of maximum electric field and minimum magnetic field and the surface is perpendicular to the electric field then another assumption can be made. Assume that the sample does not perturb the electric fields to any extent, the electric flux densities can be set equal.

$$D_0 = D_1 = D_2 \tag{1.6}$$

$$\epsilon_0\bar{E}_0 = \epsilon_1\bar{E}_1 = \epsilon_2\bar{E}_2 \tag{1.7}$$

Therefore the perturbation equations (1.4) and (1.5) can be written as

$$\frac{\Delta\omega_1}{\omega_1} \approx \frac{\frac{\epsilon_0-\epsilon_1}{\epsilon_1}\int_{vs} 2\epsilon_0|E_{0_{rms}}|^2dV}{\int (\epsilon_0\bar{E}_0\cdot\bar{E}_1-\mu_0\bar{H}_0\cdot\bar{H}_1)dV} \tag{1.8}$$

$$\frac{\Delta\omega_2}{\omega_2} \approx \frac{\frac{\epsilon_0-\epsilon_2}{\epsilon_2}\int_{vs} 2\epsilon_0|E_{0_{rms}}|^2dV}{\int_{vc} (\epsilon_0\bar{E}_0\cdot\bar{E}_2-\mu_0\bar{H}_0\cdot\bar{H}_2)dV} \tag{1.9}$$

The integrals in the right side of equations (1.8) and (1.9) are similar in that they are ratios of energy stored in the sample to that stored in the cavity. They are not easily calculated because of the difficulty in measuring the fields but may be experimentally determined as a geometric filling factor. This factor is a constant for a fixed sample size and is denoted as G. Thus equations (1.8) and (1.9) become

$$\frac{\Delta\omega_1}{\omega_1} \approx \frac{\epsilon_0-\epsilon_1}{\epsilon_1} G_1 \tag{1.10}$$

$$\frac{\Delta\omega_2}{\omega_2} \approx \frac{\varepsilon_0-\varepsilon_1}{\varepsilon_1} G_2 \tag{1.11}$$

In the integral over the volume of the cavity, it is assumed that the fields are undisturbed. Thus $\bar{E}_0=\bar{E}_1=\bar{E}_2$ and $\bar{H}_0=\bar{H}_1=\bar{H}_2$ and therefore $G_0=G_1=G_2=G$.

$$G = \frac{\int_{vs} 2\varepsilon_0 |E_{0_{rms}}|^2 dV}{\int_{vc} (\varepsilon_0 \bar{E}_0^2 - \mu_0 \bar{H}_0^2) dV}$$

$$= \frac{2\int_{vs} \varepsilon_0 |E_{0_{rms}}|^2 dV}{\int_{vc} (\varepsilon_0 Ed^2 + \mu_0 |H_0|^2) dV}$$

$$= \frac{\int_{vs} \varepsilon_0 |E_{0_{rms}}|^2 dV}{2\int_{vc} \varepsilon_0 |E_{0_{rms}}|^2 dV} \tag{1.12}$$

(Since electric fields are assumed real quantities, magnetic fields are imaginary and $\varepsilon_0|E_0|^2=\mu_0|H_0|^2$.)

The frequency change that occurs when the sample is excited is

$$\frac{\delta\omega}{\omega} \approx \frac{\Delta\omega_2}{\omega_2} - \frac{\Delta\omega_1}{\omega_1} \tag{1.13}$$

Substituting from equations (1.10) and (1.11)

$$\frac{\delta\omega}{\omega} = \varepsilon_0 G\left[\frac{1}{\varepsilon_2} - \frac{1}{\varepsilon_1}\right] \tag{1.14}$$

Arndt[5]) developed the relationship between the complex dielectric constant $\varepsilon^* = \varepsilon_0(\varepsilon' - j\varepsilon'')$ and the physical properties of semiconductors in order to predict the frequency and Q perturbations. Using a

classical free carrier treatment the differential equation relating the forces on a carrier in a semiconductor subjected to a periodic field can be written:

$$m^* \frac{dV}{dt} + \frac{m^*V}{\tau} = eEe^{j\omega t} \qquad (1.15)$$

where

$m^* \frac{dV}{dt}$ = accelerating force

m^* = effective mass of the carrier

V = velocity of the carrier

$\frac{m^*}{\tau}$ = friction force

τ = momentum relaxation time

ω = driving frequency

e = charge of the carrier

The above equation is obtained from the relation F=ma=qE with the addition of a retarding friction force due to momentum. This equation is solved for the carrier velocity and then an expression for the complex conductivity is written as

$$\sigma = \frac{ne^2}{m^*} \left[\frac{\tau}{1+\omega^2\tau^2} - j\frac{\omega\tau^2}{1+\omega^2\tau^2}\right] \qquad (1.16)$$

The complex dielectric constant can be expressed as

$$\epsilon^* = \epsilon + \frac{\sigma}{j\omega} = \epsilon_0(\epsilon_\ell + \frac{\sigma}{j\omega\epsilon_0}) = \epsilon_0(\epsilon' - j\epsilon'') \qquad (1.17)$$

where

ϵ' = real part of the dielectric constant

ϵ'' = imaginary part of the dielectric constant

ϵ_ℓ = lattice contribution to the dielectric constant

Substituting equation (1.16) into (1.17), the result is

$$\varepsilon^* = \varepsilon_0\left(\varepsilon_\ell - \frac{ne^2}{m^*\varepsilon_0}\frac{\tau^2}{1+\omega^2\tau^2} + \frac{ne^2}{j\omega\varepsilon_0 m^*}\frac{\tau}{1+\omega^2\tau^2}\right) \tag{1.18}$$

with real and imaginary parts:

$$\varepsilon' = \varepsilon_\ell - \frac{ne^2}{m^*\varepsilon_0}\frac{\tau^2}{1+\omega^2\tau^2}$$

$$\varepsilon'' = \frac{ne^2}{m^*\varepsilon_0\omega}\frac{\tau}{1+\omega^2\tau^2} \tag{1.19}$$

Thus the dielectric constant of a semiconductor decreases when the conduction electron density is increased due to photo-induced contributions.

Now the dielectric constants can be expressed as

$$\frac{\varepsilon_2}{\varepsilon_0} = (\varepsilon_\ell - kn) - j\left(\frac{kn}{\omega\tau}\right)$$

$$= (\varepsilon\ell - \varepsilon\psi) - j\left(\frac{\varepsilon\psi}{\omega\tau}\right) \tag{1.20}$$

and

$$\frac{\varepsilon_1}{\varepsilon_0} = \varepsilon_\ell \tag{1.21}$$

where

$$k = \frac{e^2}{m^*\varepsilon_0}\frac{\tau^2}{1+(\omega\tau)^2} \tag{1.22}$$

and

$$n = \frac{\alpha P_\psi \tau_L}{h\nu Vs} \tag{1.23}$$

$= $ number of optically created free carriers

$\alpha = $ conversion efficiency

$P_\psi = $ incident light power

$\tau_L = $ free carrier lifetime

h = Planck's Constant

ν = frequency of incident light

V_s = volume of sample

Equation (1.20) expresses the dielectric constant as the difference of the lattice contributions and photo-induced contributions. Thermal contributions are neglected since the work will be done in liquid helium (4.2°K).

Substituting equations (1.20) and (1.21) into equation (1.14) results in

$$\frac{\delta\omega}{\omega} = G\left[\frac{\varepsilon_\ell - \varepsilon_\psi + J\varepsilon\psi/\omega\tau}{(\varepsilon_\ell - \varepsilon_\psi)^2 + (\varepsilon\psi/\omega\tau)^2} - \frac{1}{\varepsilon_\ell}\right] \qquad (1.24)$$

Referring to equation (1.2), the real part of equation (1.24) is related to the frequency shift of the cavity. Therefore

$$\mathrm{Re}\left(\frac{\delta\omega}{\omega}\right) = G\left[\frac{\varepsilon_\ell - \varepsilon_\psi}{(\varepsilon_\ell - \varepsilon_\psi)^2 + (\varepsilon\psi/\omega\tau)^2} - \frac{1}{\varepsilon_\ell}\right] \qquad (1.25)$$

Equation (1.25) has been used[5] successfully to predict the free carrier behavior of the photodielectric effect in Si, Ge, GaAs, InAs, and InSb.

1.3 Traps and Recombination Centers

Once free carriers have been created they remain free until captured at an imperfection in the material. Generally, these capturing centers are classified into two groups: (1) trapping centers - if the probability of the carrier being re-excited is greater than that of it recombining with a carrier of opposite sign (2) recombination centers - if recombination is more probable than re-excitation.

1.4 Effects of Traps

Bube[6]) discusses three principal hypothesis to explain the photodielectric effect. (1) It is another method of measuring the photoconductivity of the material. (2) It is a real change in the dielectric constant of the material, caused by the existance of polarizable centers consisting of electrons loosely bound to traps. (3) It is a real change in the dielectric constant, but is caused by the existance of space charges at material grain boundaries.

Hinds[7]) points out that the magnitude of the photodielectric effect in CdS is directly related to the density and location of traps in the forbidden band. The first free carriers created are captured by both hole and electron traps. Soon, however, the electron traps are filled and all the electrons generated subsequently move into the conduction band. This continues until all the hole traps also become full and any holes generated are free for recombination. Figure I-1 shows the expected conduction result. During the first portion (t_0-t_1) both hole and electron traps are filling and no conduction occurs. From t_1 to t_2 conduction increases when the electron traps are filled and electrons are collected in the conduction band. At $t=t_2$ the hole traps begin to saturate and carriers generated are free for recombination.

In a very complete discussion relating to the complex dielectric constant to semiconductor properties Hinds[7]) shows that the presence of traps has a distinct influence on the relative dielectric constant. This is done by adding a term, expressing an elastic binding force, to

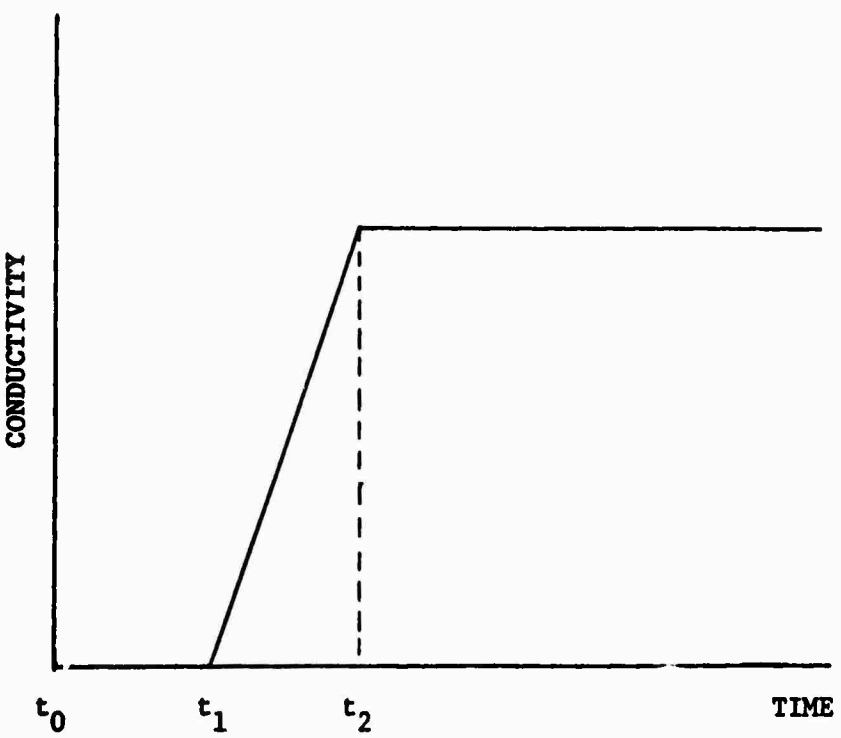

Fig. I-1 Curve of Conductivity vs Time Using Constant Light

the previously discussed equation of force on free carriers.

Equation (1.15) with this binding force added becomes

$$m^*\frac{d^2x}{dt^2} + \frac{m^*}{\tau}\frac{dx}{dt} + kx = eEe^{j\omega t} \tag{1.26}$$

where

$Ee^{j\omega t}$ = the electric field around the sample

m^* = the effective mass of the carrier

x = the displacement, in one direction, of the particle from equilibrium

τ = the momentum relaxation time

e = the charge of the carrier

The first term represents the acceleration force, the second gives the viscous damping force and the third is the elastic binding force.

Equation (1.26) is of the form required for a harmonic oscillator of frequency $\omega_0=\sqrt{k/m^*}$. The solution of this equation is

$$x = \frac{eEe^{j\omega t}}{m^*}\frac{(\omega_0^2-\omega^2-j\omega/\tau)}{(\omega_0^2-\omega^2)^2+(\omega/\tau)^2} \tag{1.27}$$

By considering surface charge densities it can be shown that the relative dielectric constant is expressed as:

$$\varepsilon_r = \frac{1}{\varepsilon_0 Ee^{j\omega t}}\sum_i e_i x_i + 1 \tag{1.28}$$

Substituting equation (1.27) into (1.28) the relative dielectric constant becomes

$$\varepsilon_r = \sum_i \frac{e_i^2}{m^*_i \varepsilon_0}\left[\frac{\omega_0^2-\omega^2-j\omega/\tau}{(\omega^2_0-\omega^2)^2+(\omega/\tau)^2}\right]_i + 1 \tag{1.29}$$

In order to simplify equation (1.29) several assumptions are made. Only the charges which effect the dielectric perturbation due to light are considered and all others are dropped from the summation. Therefore only a few electrons, having the same mass m_i^* and charge e_i, need be considered and these terms are taken outside the sum. The remaining electrons which do remain inside the summation can be classified into selective groups such as free, captured in deep traps, or in shallow traps. These groups are represented by a new index J and $\Delta\varepsilon_r$ is written

$$\Delta\varepsilon_r = \frac{e^2}{m^*\varepsilon_0} \sum_J \Delta n_J \left[\frac{\omega_0^2-\omega^2-j\omega/\tau}{(\omega_0^2-\omega^2)^2+(\omega/\tau)^2}\right]_J \tag{1.30}$$

where Δn_J represents the net change in the density of electrons in the J-th group. Writing equation (1.30) in real and imaginary parts.

$$\Delta\varepsilon_r = \Delta\varepsilon_r' - \Delta\varepsilon_r''$$

and

$$\Delta\varepsilon_r' = \frac{e^2}{m^*\varepsilon_0} \sum_J \Delta n_J \left[\frac{\omega_0^2-\omega^2}{(\omega_0^2-\omega^2)^2+(\omega/\tau)^2}\right]_J \tag{1.31}$$

$$\Delta\varepsilon_r'' = \frac{e^2}{m^*\varepsilon_0} \sum_J \Delta n_J \left[\frac{\omega/\tau}{(\omega_0^2-\omega^2)^2+(\omega/\tau)^2}\right]_J \tag{1.32}$$

Again considering the classical oscillator it can be shown that

$$\omega_0^2 = 1.70\times10^{29}\left(\frac{m}{m^*}\right)E^3(eV) \tag{1.33}$$

where E(eV) is the binding energy expressed in electron-volts. Based upon equations (1.31) and (1.33) the relation of E and $\Delta\varepsilon_r'$ can be noted. For a constant ω, different simplifications of $\Delta\varepsilon_r'$ can be obtained as the binding energy is varied. When $\omega_0 >> \omega$, the bracketed

term in equation (1.31) may be replaced by $(1/\omega_0)^2$ and thus $\Delta\varepsilon_r'$ increases as E decreases. Now let $\omega/\tau > \omega_0^2$, $\Delta\varepsilon_r'$ decreases as E decreases and

$$\Delta\varepsilon_r' \quad \alpha\left[\frac{\omega_0^2}{(\omega/\tau)^2}\right] \tag{1.34}$$

As $(\omega_0^2-\omega^2)$ changes from positive to negative, $\Delta\varepsilon_r'$ becomes zero and then negative and may be expressed as

$$\Delta\varepsilon_r' \quad \alpha\left[\frac{\omega_0^2-\omega^2}{(\omega/\tau)^2}\right] \tag{1.35}$$

Finally when $\omega >> \omega_0$, ε_r' remains negative and the bound electron takes on the characteristics of a free carrier. For this case the equation is identical to that obtained earlier for free electrons.

$$\Delta\varepsilon_r' = -\frac{ne^2}{m^*\varepsilon_0}\frac{\tau^2}{1+\omega^2\tau^2} \tag{1.36}$$

1.5 Traps in Amorphous Semiconductors

In the previous sections it is pointed out that in many materials the photodielectric effect has been exhibited due to the presence of traps. Therefore it is suspected that various amorphous semiconductors should also show some photodielectric effect since the models that have been hypothized place many trapping sites in the forbidden band.

Cohen[8]) has applied the effects of trapping sites to the amorphous semiconductor model developed by Cohen, Fritzsche and Ovshinsky[9]). Andriesh and Kolomiets[10]) report the presence of current carrier trapping centers in the forbidden band of the amorphous semiconductor $Tl_2Se \cdot As_2Te_3$. Also multiple trapping levels are reported in the

amorphous chalcogenide alloy As(50%)-Te(30%)-Ge(11%)-Si(9%) by Botila and Vancu[11]). Kolomiets, Ljubin and Averjanov[12]) describe the existance of both trapping sites and recombination centers in As_2Se_3.

Fagen and Fritzche[13]) explain the band model for covalent amorphous alloys which was proposed by Cohen, Fritzche, and Ovshinsky[9]). The important characteristics are a high density of localized states, shown in figure I-2 as tails from either band,and mobility edges E_v and E_c separating the localized and extended states of the conduction and valence bands, respectively. These tails overlap near the center of the mobility gap and cause electron hopping from upper valence band states to lower conduction band states. During steady-state irradation, E_F^0 splits into electron and hole quasi-Fermi levels, E_F^e and E_F^h . When the energy source is removed, the photo-excited carriers may recombine through the recombination centers located between the electron and hole quasi-Fermi levels. This accounts for the fast component of decay of photoconductivity that has been reported[9]). During this fast decay, the quasi-Fermi levels move partly back toward equilibrium. The slow component of decay of photoconductivity, that is reported with the fast decay, suggests a relaxation process of phonon-assisted tunneling between spatially separated localized states.

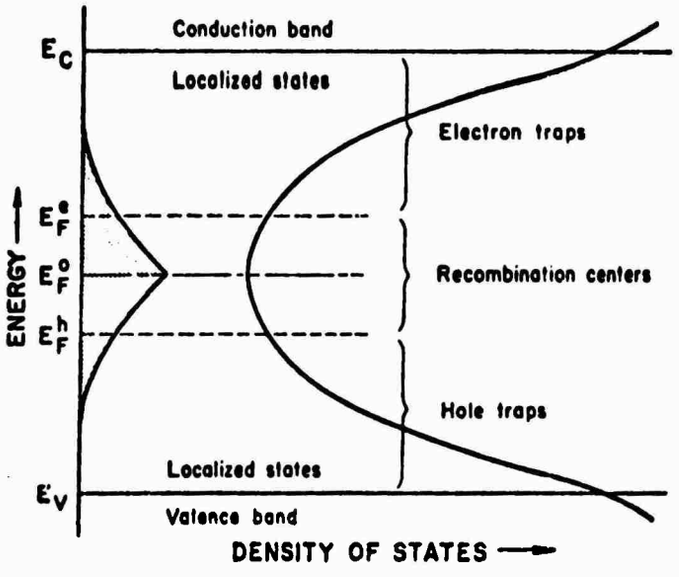

Fig. I-2 Band Model for Amorphous Alloys

CHAPTER II

EQUIPMENT AND EXPERIMENTAL TECHNIQUES

Many of the experimental techniques associated with the observation of the photodielectric effect in an x-band resonant cavity have not previously been established in the Physical Electronics Laboratory. Therefore methods of material processing of amorphous compounds, use of cryogenic techniques and operation of microwave equipment will be discussed fully.

2.1 Amorphous Material Processing

The amorphous compound $2As_2Se_3 \cdot As_2Te_3$ is made in a specially designed oven in the Amorphous Semiconductor Laboratory. This oven is housed in an airtight enclosure to avoid contamination of the room by a possible explosion of the ampoule containing poisonous material. A rocking motor is also attached to the furnace in order to mix the constituents while the material is molten.

The material was made by combining two binaries, As_2Se_3 and As_2Te_3, in the desired proportions. The correct amount of each of these was weighed on an analytical balance and then loaded into a vycor tube. This was then evacuated and sealed using an oxy-hydrogen torch. The sealed amouple was then inserted into the overn (preheated to 800°C) and allowed to remain for 8 hours. During the last hour in the oven the sample was agitated by rocking to assure a uniform mixture of all components. At the end of the 8 hour period the ampoule was removed and allowed to quinch slowly at room temperature. The sample

hardened into a solid ingot which was extracted by breaking the glass capsule.

2.2 Sample Preparation

In order to obtain a sample for use in the photodielectric measurements, the ingot was sawed into wafers approximately 2 mm thick using a jewlers saw. A fine grit sandpaper was used to lap the surfaces smooth. In order to attach the prepared sample to the teflon holder several adhesives were tried but Duro epoxy cement was found to be the most satisfactory.

2.3 The Cryogenic System

The dewar system. In order to maintain a cryogenic environment, the dewar system shown in figure II-1 is used. The evacuated envelope serves as a divider between the outer dewar containing liquid nitrogen and the inner dewar containing liquid helium.

The circuit, a resonant cavity, is suspended at the end of the stainless steel waveguide and is aligned with the lenses in both the inner and outer dewar. The light is introduced through a small hole in the cavity via these lenses. The plate which holds the waveguide rigid in the dewar can be unbolted from the header assembly to allow easy removal of the waveguide and cavity. The "O" ring seal around the header opening and a mica strip in the waveguide joint provide vacuum tight seals.

Pre-cooling procedure. In order to cool the dewars and the circuit properly, a systematic method must be followed. The dewars must

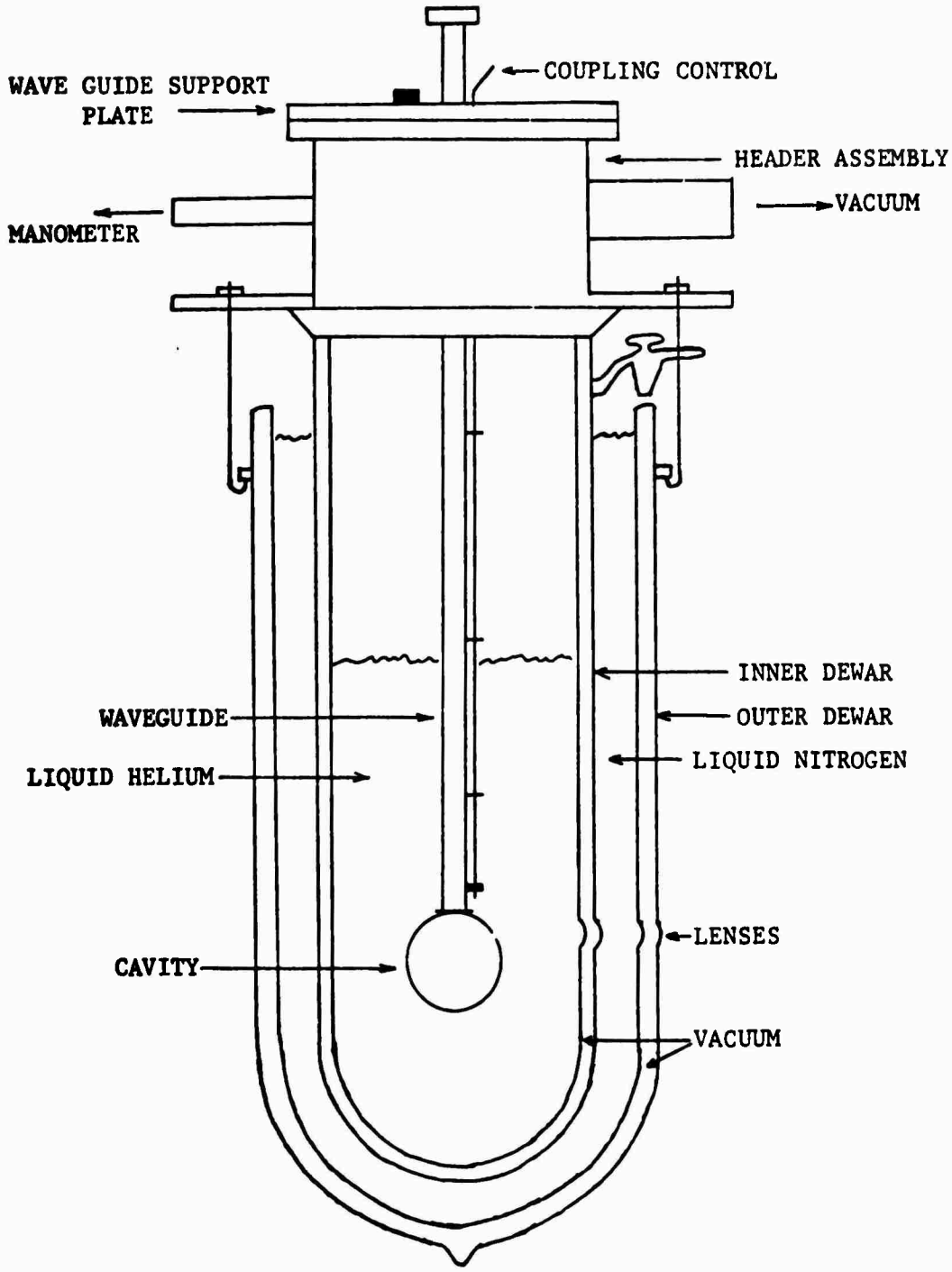

Fig. II-1 Dewar System

be clean and completely dry before the procedure is begun. First the envelope of the inner dewar must be pumped out completely in order to prevent ice from thermally shorting the liquid helium to the ambient. Next the inner dewar is evacuated and held until it is time to transfer liquid helium. Liquid nitrogen is now transfered into the outer dewar to start the cooling process and is allowed to stand for approximately eight hours. This period allows the inner dewar and the circuit it contains to cool approximately to liquid nitrogen temperature (77°K). The vacuum on the inner dewar should be removed by pressurizing it to room pressure with helium gas. Care must be used to prevent any air to enter the dewar during this stage of the procedure. Liquid helium is then transfered by standard techniques.

2.4 Microwave Equipment

Many different pieces of microwave apparatus were integrated into the system, used as a tool to examine the amorphous compound. Figure II-2 shows the arrangement of the complete system.

Resonant Cavity. A TE-011 cylindrical cavity is used to house the sample. The currents in this mode are circular in the end plates thus no current crosses a mechanical joint. This preserves the inherent high Q of the cavity. Also the TE-011 mode produces zero electric field everywhere on the surface, therefore the coupling from the

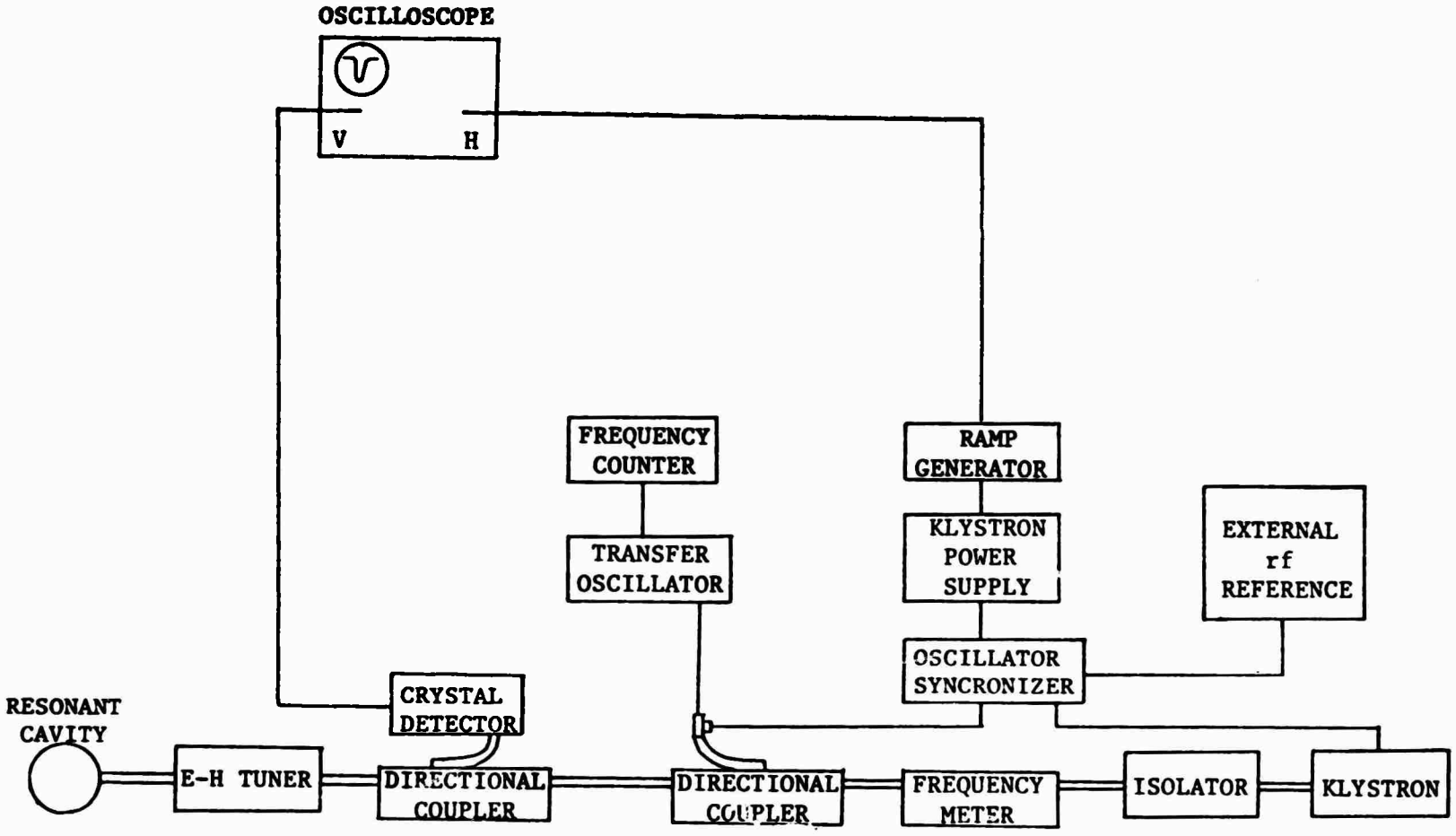

Fig. II-2 Microwave System

waveguide into the cavity is chosen to be magnetic for convenience. This is accomplished with an iris opening in the cylinder wall and a small wire loop mounted on a teflon holder. The plane of the loop is parallel with the short side of the waveguide. The wire can be moved in and out of the iris, thus varying the position of the loop in the TE-10 field pattern of the rectangular guide and the amount of coupling into the cavity. Figure II-3 shows the cavity-waveguide configuration with the sample in the position of maximum electric field and the loop for magnetic coupling.

The field equations for a cylindrical resonator in the TE-011 mode can be derived from Maxwell's equations

$$\bar{\nabla} \times \bar{E} = -j\omega\mu\bar{H} \tag{2.1}$$

$$\nabla \times \bar{H} = j\omega\varepsilon\bar{E} \tag{2.2}$$

and the wave equation in cylindrical coordinates

$$\frac{\partial^2 Hz}{\partial r^2} + \frac{1}{r}\frac{\partial Hz}{\partial r} + \frac{1}{r^2}\frac{\partial^2 Hz}{\partial \phi 2} = -k_c{}^2 Hz \tag{2.3}$$

where

$$k_c{}^2 = \gamma^2 + \omega^2\mu\varepsilon$$

By manipulating the above equations and applying the boundary condition that the tangential electric field must be zero the following field equations are obtained for the TE-011 cavity.

$$H_z = -J2AJ_0(r\frac{P_{01}}{a})\sin\frac{\pi}{d}z \tag{2.4}$$

$$E_\phi = 2An\frac{f}{fc}J_0'(r\frac{P_{01}}{a})\sin\frac{\pi}{d}z \tag{2.5}$$

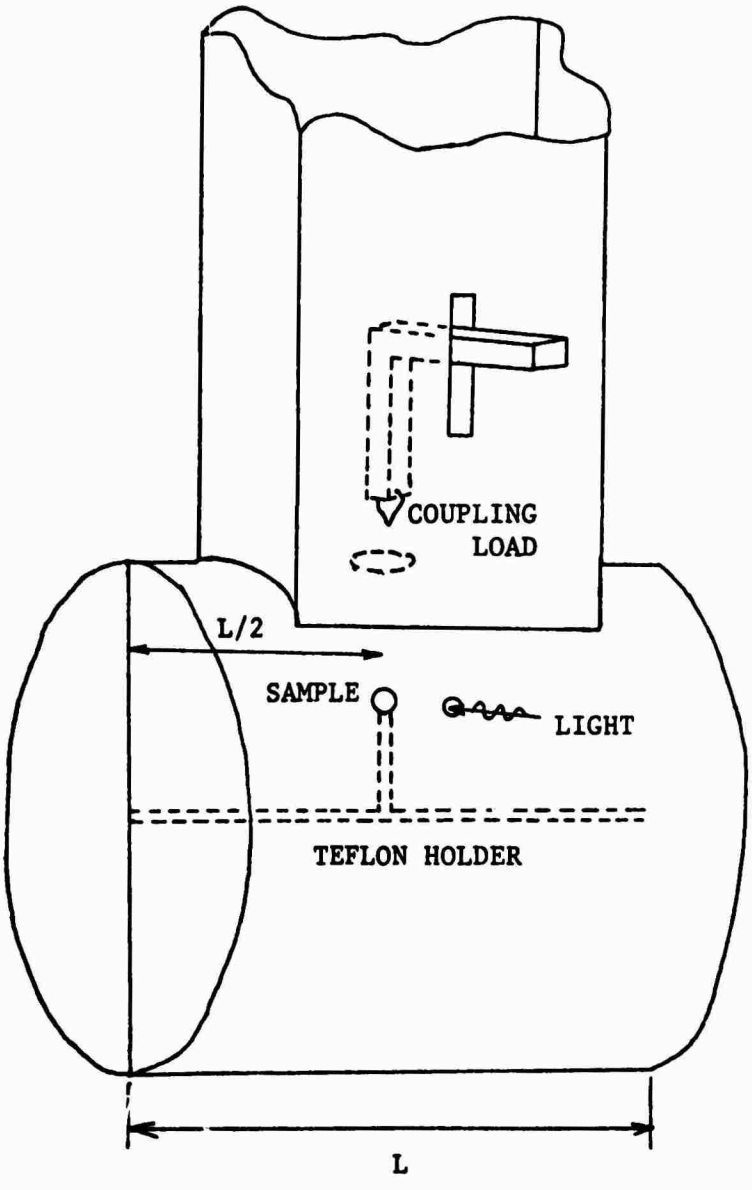

Fig. II-3 Cavity-Waveguide Configuration

$$H_r = -2A \frac{\eta}{Z_{TE}} \frac{f}{fc} J_0'(r \frac{P_{01}}{a}) \cos \frac{\pi}{d} z \qquad (2.6)$$

where

d = length of the cavity along z axis

$Z_{TE} = \eta[1-(\frac{fc}{f})^2]^{-1/2}$

$\eta = \sqrt{\frac{\mu}{\epsilon}}$

P_{01} = 3.81 (the first root $J_0'(x)=0$)

r = radius of the cavity

fc = cutoff frequency

Klystron. A Varian X-13 reflex klystron with a frequency range of 8.1 to 12.4 GHz. is used as the microwave source. The klystron is powered by a Hewlett Packard Model 715A power supply.

Oscillator Syncronizer. The oscillator synchronizer is used to stabilize the klystron frequency which is prone to drift from its original setting. The instrument used is a Hewlett Packard Model DY-2650A which operates on the principle of automatic phase control (APC). A small sample (approximately -10dbm) of the klystron's signal is mixed with a harmonic of the signal from a temperature-stabilized crystal rf reference oscillator, either internal or external, to produce a 30 MHz i-f signal. This i-f signal is then phase compared to an i-f reference signal from an internal or external source. After the frequency is "locked", any attempts by the klystron to shift frequency produce a phase error and a phase comparator output error voltage. This voltage is applied in series with the

klystron's repeller voltage to correct the frequency shift.

Transfer Oscillator. The Hewlett-Packard Model 540B Transfer Oscillator is utilized to extend the range of the electronic counter into the x-band range of frequencies. The method used to determine frequency is to zero-beat the unknown input signal with a harmonic of an extremely stable signal generated internally and measure the low frequency of the harmonic on the counter.

2.5 Frequency Measurements

Measuring the exact resonant frequency of the TE-011 cavity required the use of the equipment discussed previously. In order to determine the frequency shift due to the change in the dielectric constant of the sample, the resonant frequency must be measured both before and after exciting the material.

The first step in frequency measurements is to obtain a mode pattern of the klystron on the oscilloscope. This is accomplished by modulating the klystron with a ramp signal and also using this ramp to drive the horizontal sweep of the scope. The resulting pattern is shown in figure II-4. Next, the klystron is tuned to find the cavity resonance which is manifested as a small dip in the mode pattern since the cavity is operated in the reflection mode rather than transmission mode. This dip should be placed at the top of the mode pattern as is shown in figure II-5, by tuning the klystron and the repeller voltage.

The klystron should then be placed in the cw mode and the ramp signal removed from the oscilloscope. This procedure will cause a

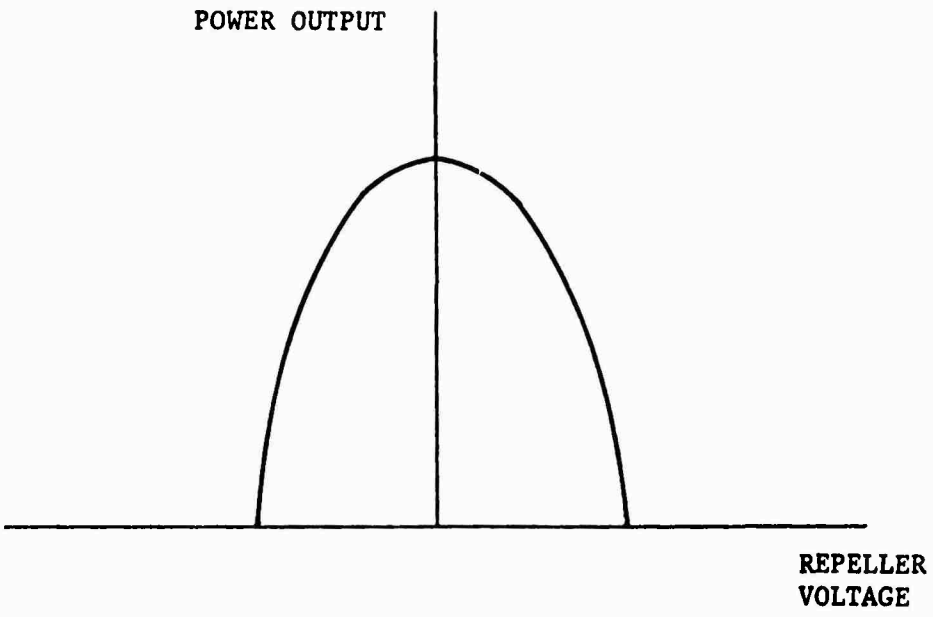

Fig. II-4 Klystron Mode Pattern

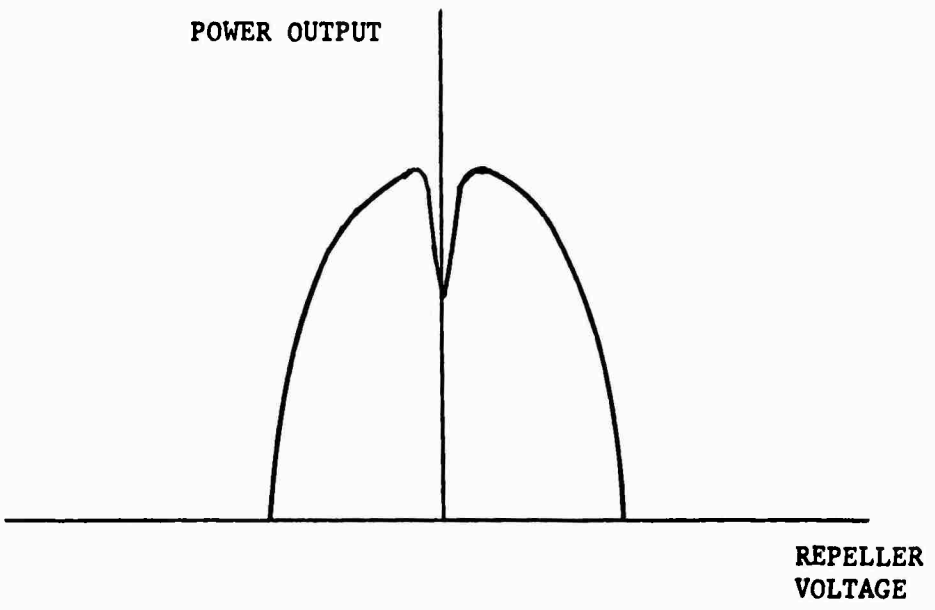

Fig. II-5 Resonant Frequency Dip

single dot to appear on the scope. This is an unswept representation of the mode pattern and dip explained above. To tune the klystron to the exact resonant frequency of the cavity the repeller voltage should be adjusted to move the dot to the bottom of the dip.

Normally the frequency of the klystron is prone to drift from the desired setting so some type of stabilization is required. The klystron frequency is "locked" using the oscillator syncronizer discussed earlier. The APC switch on the syncronizer is turned to the on position and the klystron is locked by adjusting the external rf reference source (General Radio Oscillator, type 1208-B) until the search light goes out. The dot will now have to be returned to the bottom of the dip by adjusting the rf reference and VFO controls. Often it is not an easy matter to re-tune for resonance using the external rf reference and several attempts are usually necessary before the dot can be tuned to the desired point without loosing "lock".

The klystron is now tuned and locked to the exact resonant frequency of the cavity. This frequency is measured using the wavemeter, transfer oscillator and frequency counter. The frequency can be measured to two decimal places by tuning the wavemeter until its dip coincides with the cavity, causing the dot to drop further on the scope face. Then the transfer oscillator is tuned to a convenient fundamental frequency of that measured on the wavemeter. When this is reached a vertical deflection will be seen on the internal crt. The gate control on the counter should now be set to the external reset position so that the counter will measure the transfer oscillator

fundamental frequency at the precise moment that zero beat is reached. Now the fine vernier control should be tuned to reduce the difference-frequency to as close to zero as can be obtained. At the instant the zero beat is obtained, the counter reset button should be pressed to measure and record the frequency.

2.6 Optical Excitation

A He-Ne gas laser, LAS-2002, from Electro Optics Associates, was used to excite the amorphous sample. This laser produced light with a wavelength of 6328Å at a power of approximately 0.5 milliwatts. This wavelength corresponds to an energy of 1.965×10^3 meV. A projector lamp was also used as a white light source when a more powerful light source was needed.

In order to prevent unwanted light from exciting the sample prematurely, the dewar system was covered and a camera shutter was aligned with the lenses to provide precise control of the light.

2.7 Measurement of Cavity Q

In order to determine that the sample is effectively dominating the cavity, it is necessary to measure the Q of the empty cavity, and compare that to measurements of the Q of the cavity loaded with the teflon holder only and with the sample on the holder. A method developed by Ashley and Palka[14]) is used to make these Q measurements. The apparatus is assembled as shown in figure II-6 with the forward and reflected wave channels each connected to a vertical amplifier and the sweep output of the generator connected to the horizontal input. The

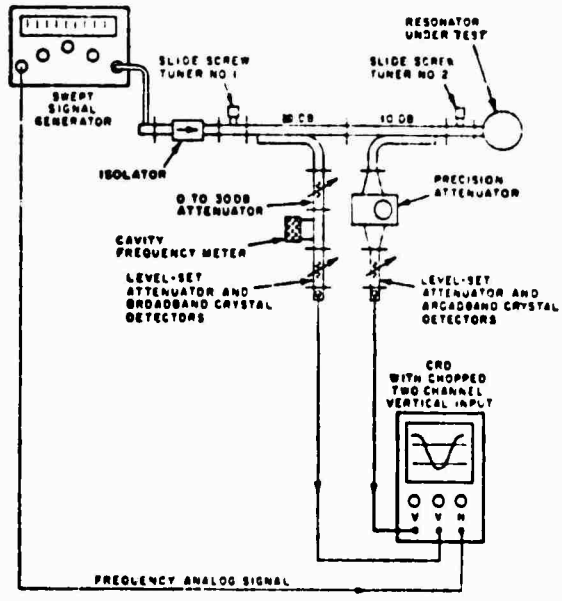

Fig. II-6 Apparatus for Q Measurement

apparatus is assembled as shown in figure II-6 with the forward and reflected wave channels each connected to a vertical amplifier and the sweep output of the generator connected to the horizontal input. The oscilloscope is used in the chopped mode.

The sweep generator is adjusted to sweep through resonance and far enough on either side to present a complete view of the resonance dip. Slide screw tuner no. 1 is now adjusted so that no small dips or peaks appear in the incident wave. The vertical inputs to both channels are now grounded so that both levels can be adjusted to a common reference. Then the inputs are placed in the dc coupled mode and the two level-set attenuators just ahead of the detector mounts are set to equalize the detector outputs with the test resonator replaced by a good short.

With the precision attenuator set to zero, the incident wave attenuator is adjusted to position the reference line at the bottom of the resonator dip. (Figure II-7a.) Now the precision attenuator is adjusted until the line from the resonant channel coincides with the line from the incident channel as shown in figure II-7b. The sweep generator may have to be tuned slightly off of resonance so that the flat top of the mode may be used in this alignment. The setting on the precision attenuator is a measurement of the reflection coefficient at resonance.

This value is now placed on the abscissa of figure II-8 and another setting of the attenuator is read off the ordinate. The new setting will determine the half power bandwidth of the resonator.

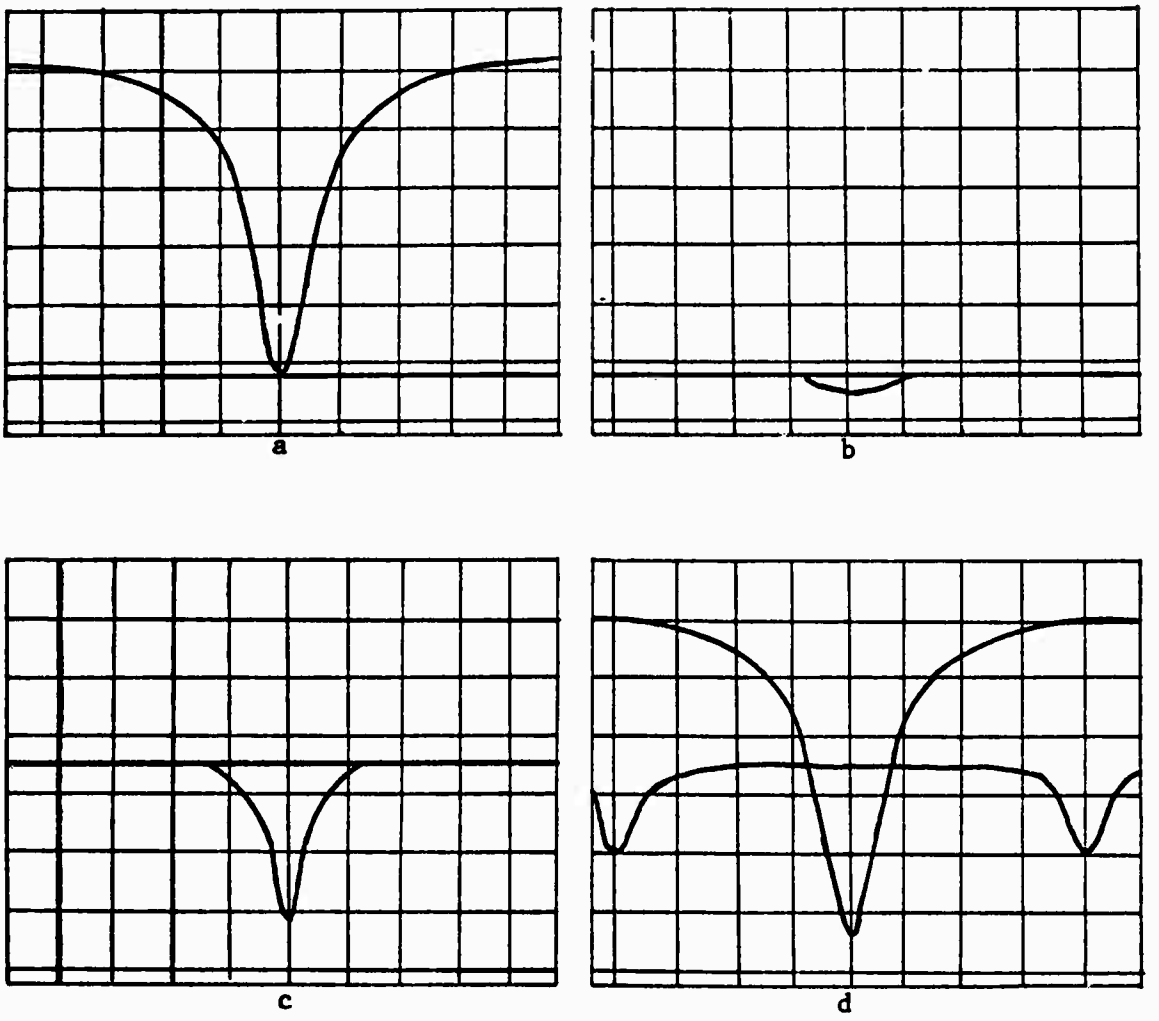

Fig. II-7 Oscilloscope Presentation of Q Data

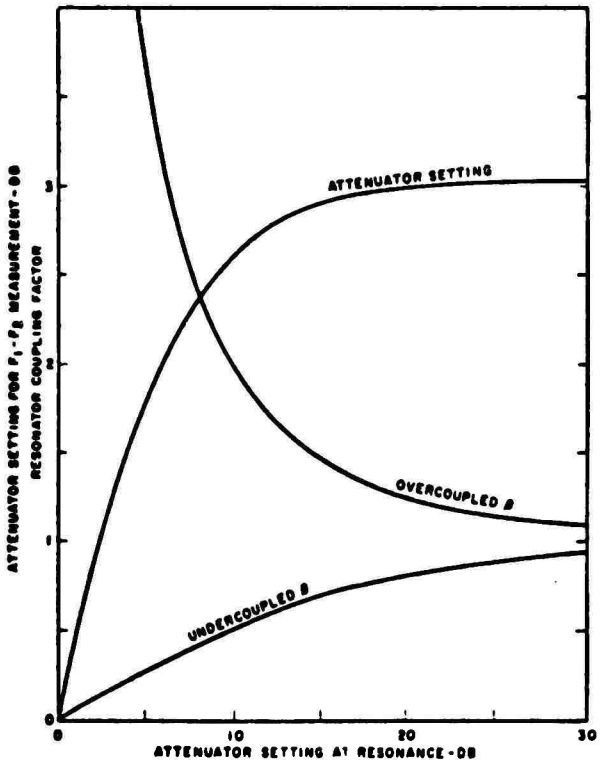

Fig. II-8 Beta and Attentuator Settings

The precision attenuator is set to this new attenuation value and the forward wave channel attenuator is adjusted so that both reference lines coincide as shown in figure II-7c. Then all attenuation is removed from the reflected channel by returning the precision attenuator to zero dB. Figure II-7d shows the reflected channel dip, with all attenuation removed, and the forward wave channel crossing it. Now the bandwidth f_2-f_1 of the resonator is measured between the two crossings of the dip by the forward channel.

The oscilloscope screen grid is now calibrated in frequency so that the bandwidth can be read directly. This is accomplished by using the frequency meter to measure the total frequency change for 8 divisions along the horizontal (figure II-7d). If the analog voltage of the sweep generator is directly proportional to frequency over this limited range, then a simple measurement of length gives f_2-f_1.

Now the loaded Q is calculated as

$$Q_L = \frac{f_0}{f_2-f_1} \tag{2.7}$$

where f_0 is the resonant frequency of the resonator.

To determine the unloaded Q of the cavity, Q_0, knowledge of the coupling factor β is required. However in this method of Q determination, it is sufficient to know only whether the cavity is overcoupled or undercoupled. Slide screw tuner no.2, just ahead of the cavity, is used to determine this information. This tuner is adjusted until the reflection at resonance is small and then the tuner probe is with-

drawn. If the bandwidth of the resonator decreases as the probe is removed, the cavity is undercoupled; but if the bandwidth increases, the cavity is overcoupled.

Using this information about coupling and the original precision attenuator setting, the value of β can be determined from figure II-8. This value of β is substituted into the following equation and the value of the unloaded Q is calculated.

$$Q_0 = (\beta + 1)\, Q_L \qquad (2.8)$$

CHAPTER III

RESULTS AND CONCLUSIONS

Several different samples of $2As_2Se_3 \cdot As_2Te_3$, As_2Se_3, As_2Te_3, As_2S_3 and Si(3%) Ge(4%) As(38%) Te(55%) were used in the photodielectric tests. These varied in size from about 0.3cm in diameter and 0.1cm thick to 0.75cm in diameter and 0.3cm thick. The G factors of these samples ranged from 0.00176 to 0.015. The experiment, as described in the previous chapter, was performed on these samples at room temperature, liquid nitrogen temperature (77°K) and liquid helium temperature (4.2°K), however, no photodielectric effect was observed.

In order to establish that the apparatus was not at fault, an Al doped sample of CdS, known to exhibit the photodielectric effect at 900 MHz, was tested. The equipment performed properly and a frequency shift of 1.61 MHz was observed for full illumination from the HeNe laser. Q measurements were also conducted as described in the previous chapter, and it was determined that the sample dominated the loaded cavity. Thus any change in the sample polarization would be directly observable as a change in the resonant frequency, and any conductivity change would be reflected in the loaded Q of the cavity. In addition to establishing the integrity of the electronics, the alignment of the optics from the ambient, through the liquified gases, into the cavity was verified.

In order to determine the general structure of the tested

materials, X-ray diffraction methods were used. The results showed a generally disordered structure with some short range order existing. This data agrees with the existing theories which postulate the lack of long range order and the presence of some short range order in these types of materials.

Based on the negative results for the five amorphous materials tested, it is premature to postulate the lack of a photodielectric effect to be a universal feature of disordered materials. However, it is appropriate to investigate known material properties of the amorphous chalcogenides to determine if some common denominator exists that would explain the apparent lack of depolarization. Therefore, this chapter discusses several possible explanations based upon the limited amount of data and partial theories that do exist.

3.1 Optical Absorption

Optical data on the material $2As_2Se_3 \cdot As_2Te_3$ is not available, but several authors give optical absorption and photoconductivity measurements for As_2Se_3, As_2Te_3, Te and Se. Rockstad[15]) measures an energy gap of 1.75eV in As_2Se_3 by optical methods and shows absorption data (figure III-1) for this and related materials. Davis and Shaw[16]) report data on amorphous As_2Se_3, Se and Te as shown in figure III-2. These curves suggest that photon energy between 1.0 and 2.0eV might be used to excite the material under study. Edmond[17]) also reports optical absorption data on As_2Se_3 which supports these findings.

Optical absorption data is given by Fagen and Fritzsche[18]) on an

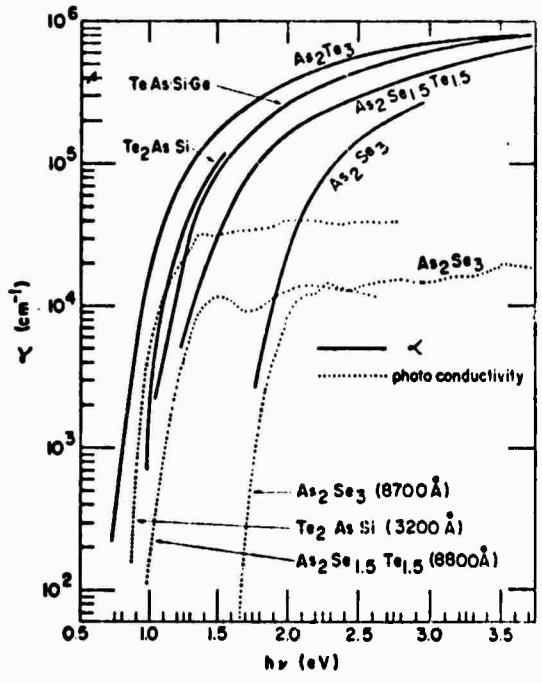

Fig. III-1 Optical Absorption Coefficient (ref. 15)

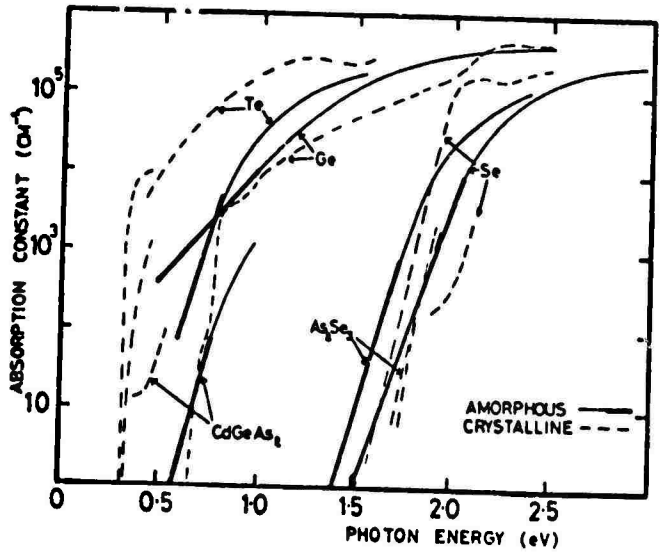

Fig. III-2 Optical Absorption Edges for As_2Se_3 (ref. 16)

amorphous material of the formula: Si(11%) Ge(11%) As(35%) P(3%) Te(40%) (type A material). Since this compound is predominately As and Te, the optical data should be applicable to the material under observation. Figure III-3 shows absorption data for the type A material which agrees with the reports of other authors on As_2Se_3. Figure III-4 also suggests the use of photons of energy greater than 1.0eV.

From the above optical absorption data, it is seen that the photon energy of the 6328 Å Laser light (~1.95eV) might have been marginal for band to band transitions in many of the materials. Therefore, a mercury arc lamp, containing lines from 1850 Å to 5461 Å, was used in duplicate tests. However these tests also failed to show any positive results.

Although sufficiently energetic photons were provided for band to band transitions or localized state to band transitions, there is uncertainty as to the number of created polarizable centers. In particular, if the available states in the forbidden band are considered, optical absorption data[19]) predicts an upper limit of $10^{16}eV^{-1}cm^{-3}$ gap states. However contradictory electrical data[19]) sets the density of gap states at $10^{19}eV^{-1}cm^{-3}$ in order to explain the lack of a field effect in several chalcogenides[19]). If the worse case condition is chosen, the density of states would be marginal for observation of polarization changes based on sensitivity predictions for the apparatus used by Hartwig and Hinds[2]). In addition, if the majority of the trapping sites are located deep in the forbidden band, Hartwig and Hinds show that the contributions to depolarization are small since

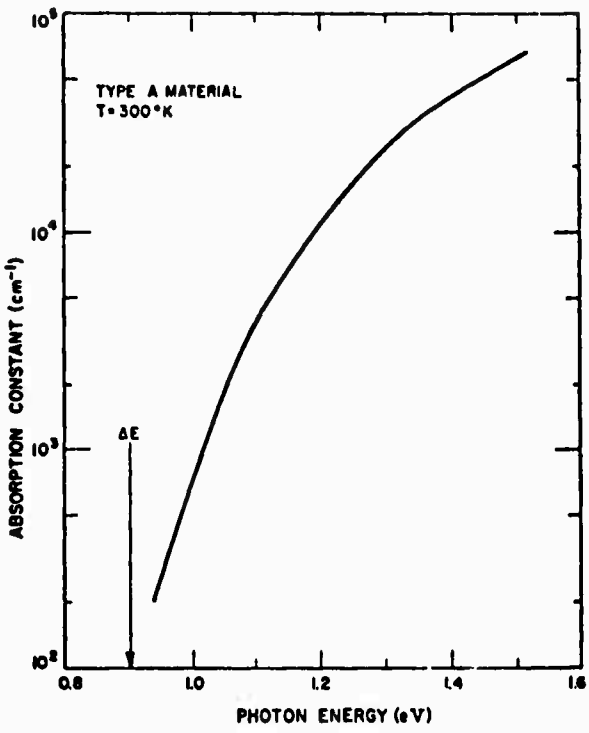

Fig. III-3 Absorption Constant for Type A Material (ref. 18)

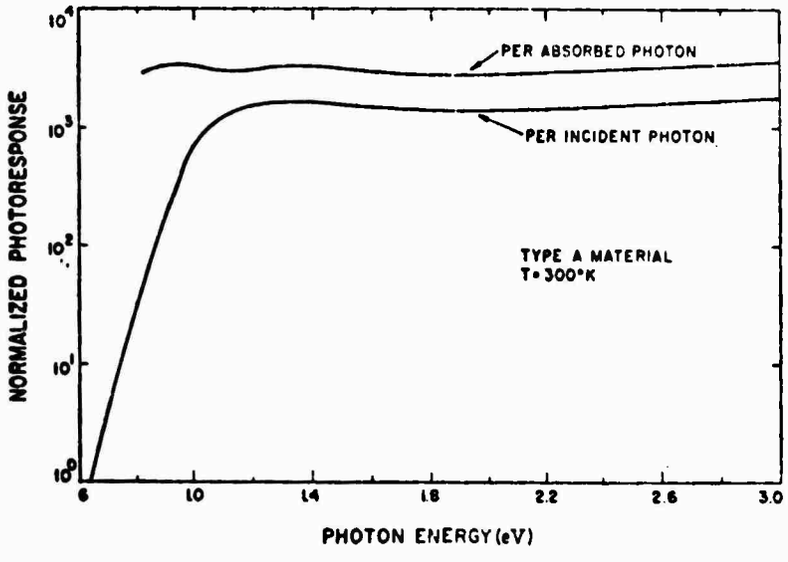

Fig. III-4 Photoresponse for Type A Material (ref. 18)

the less tightly bound traps can provide larger orbital changes and thus effect depolarization to a greater extent.

Another possibility exists if the photon intensity is too low. If all created free carriers were used to fill the deep traps without ever saturating the less polarizable centers, then there would be no observable photodielectric effect nor would there be a Q change since there would be no conduction current to change the losses in the material. Because there is no charge injected in this electrodeless experiment, the contradictory observation of photoconductivity (with carrier injection) in the materials without a corresponding Q change when the material is in the cavity, is explained. Before these suppositions can be proved or disproved, detailed thermally stimulated conductivity experiments will have to be performed to determine the trapping dynamics which are present.

3.2 Mobility Considerations

Benedict and Shockley[20]) describe the change in the real part of the dielectric constant by the equation

$$\epsilon' = \epsilon_\ell - \frac{ne^2}{\epsilon_0 m^*} \frac{1}{[(e/m^*\mu)^2 + \omega^2]} \qquad (3.1)$$

where

ϵ_ℓ = the lattice dielectric constant
n = thermally generated carrier density
e/m*= electron charge to effective mass ratio
ω = driving frequency
μ = mobility of free carriers

In analyzing the above equation it is evident that if the mobility of the free carriers is sufficiently low, then no dielectric change will be observed. Edmond[21]) suggests that in materials in the system $As_2Se_3 \cdot As_2Te_3$ there may be local fluctuations in the ratio of As_2Se_3 to As_2Te_3 causing a lowering of the effective mobility. Kolomiets and Lebedev[22]) and Hartke[23]) report that electron drift mobility in amorphous Se is lowered by the addition of a few atomic percent As or Te. Owen and Robertson[24]) show the low hole mobilities for As_2Se_3 for fields ranging from 9.4×10^4 to 55×10^4 V/cm (figure III-5).

3.3 Momentum Relaxation Time

Equations (1.19) and (1.31) show the importance of the carrier momentum relaxation time in determining the magnitude of the depolarization when the process is due to free carriers or trapping. Stone[3]) has shown that the excitation frequency-relaxation time product must be greater than or approximately equal to unity for sufficient interactions of the created charge (free or bound) with the applied field. If $\omega\tau << 1$, then little or no photodielectric effect is observed. For an excitation of $\omega = 2\pi\ (11.8)10^{10}$, $\tau \leq 10^{-12}$sec. would be sufficient to negate the photodielectric effect. Such a range of relaxation times in disordered materials is certainly reasonable since values of 10^{-12} sec. for intrinsic crystalline silicon at room temperature are typical. Furthermore, the absence of an electron spin resonance

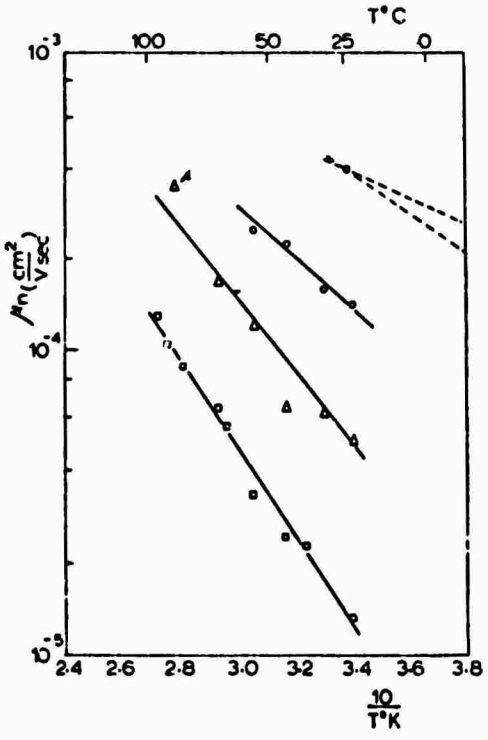

Fig. III-5 Drift Mobility for Holes in As_2Se_3 (ref. 23)

signal (sensitivity of $10^{17} cm^{-3}$) from chalcogenide films is attributed, by Fritzsche[19], to a short relaxation time, although no values are quoted.

3.4 Recomendations for Further Study

The energy levels of the trapping centers present in the energy gap can be determined more precisely by detailed thermally stimulated conductivity experiments. The observed parameter in TSC measurements is the temperature dependent electrical conductivity. The proceedure, outlined by Pickard and Davis[25], employs photon excitation, at low temperatures, to generate free carriers which can be captured by trapping centers. After photon excitation the material is heated and the electrical conductivity is monitored as a function of the temperature. During the heating cycle, the bound carriers are freed from the traps, and the current measured in excess of the dark current is defined as the thermally stimulated current. Discrete trapping levels are indicated by the presence of peaks in the thermally stimulated current vs temperature curves. These peaks can be further analyzed to give information about the trap depth in the energy, the capture cross section of the trap, and the density of trapping centers.

For future X-band frequency measurements, a plug in frequency extender for the electronic frequency counter should be obtained to replace the transfer oscillator. The method of zero-beat was found to be unreliable for measuring frequency changes of less than 0.1 MHz.

Also, the practice of maintaining the exact resonant frequency while tuning for zero-beat was experimentally inaccurate because an exact zero-beat could only be approximated.

Additional optical equipment should be added to make the total apparatus adaptable to various different types of materials, both amorphous and crystalline. Also, a more sophisticated klystron power supply, providing internal ramp modulation, would simplify the experimental proceedure and allow a whole mode pattern to be displayed on the oscilloscope at one time.

The existing microwave system, with these modifications, can be used as an effective tool to study the optical properties of many different semiconductor materials.

REFERENCES

1) G. D. Arndt, W. H. Hartwig and J. L. Stone, J. Appl. Phys. 39 (1968) 2653.

2) W. H. Hartwig and J. J. Hinds, J. Appl. Phys. 40 (1969) 2020.

3) J. L. Stone, Ph.D. Dissertation, University of Texas (1968).

4) M. Sucher and J. Fox, Handbook of Microwave Measurements (Interscience Publishers, New York, 1963).

5) G. D. Arndt, Ph.D. Dissertation, University of Texas (1966).

6) R. H. Bube, Photoconductivity of Solids (Wiley, New York, 1960).

7) J. J. Hinds, Master's Thesis, University of Texas (1968).

8) M. H. Cohen, J. Non-Crystalline Solids 2 (1970) 432.

9) M. H. Cohen, H. Fritzsche, S. R. Ovshinsky, Phys. Rev. Letters 22 (1969) 1065.

10) A. M. Andriesh and B. J. Kolomiets, Soviet Phys.- Solid State 5 (1963) 1063.

11) J. Botila and A. Vancu, Mater. Res. Bull. 5 (1970) 925.

12) B. J. Kolomiets, V. M. Ljubin and V. L. Averjanov, Mater. Res. Bull. 5 (1970) 655.

13) E. A. Fagen and H. Fritzsche, J. Non-Crystalline Solids 2 (1970) 180.

14) J. R. Ashley and F. M. Palka, The Microwave Journal 14 (1971) 35.

15) H. K. Rockstad, J. Non-Crystalline Solids 2 (1970) 192.

16) E. A. Davis and R. F. Shaw, J. Non-Crystalline Solids 2 (1970) 406.

17) J. T. Edmond, Brit. J. Appl. Phys. 17 (1966) 979.

18) E. A. Fagen and H. Fritzsche, J. Non-Crystalline Solids 4 (1970) 480.

19) H. Fritzsche, J. Non-Crystalline Solids 6 (1971) 49.

20) T. S. Benedict and W. Shockley, Phys. Rev. 91 (1953) 1565.

21) J. T. Edmond, J. Non-Crystalline Solids 1 (1968) 39.

22) B. T. Kolomiets and E. A. Lebedev, Soviet Phys.- Solid State 8 (1966) 905.

23) J. L. Hartke, Phys. Rev. 125 (1962) 1177.

24) A. E. Owen and J. M. Robertson, J. Non-Crystalline Solids 2 (1970) 40.

25) P. S. Pickard and M. V. Davis, J. Appl. Phys. 41 (1970) 2636.